FLUIDIC FLEXIBLE MATRIX COMPOSITES FOR AUTONOMOUS STRUCTURAL TAILORING

Final Report (October 1, 2006 – June 30, 2008)

AFOSR Grant Number: FA9550-07-1-0001

Submitted to:
Dr. Les Lee
AFOSR/NA
Tele: (703) 696-8483
DSN 426-8483
FAX (703) 696-8451
E-Mail: les.lee@afosr.af.mil

Principal and Co-Principal Investigators

K. W. Wang
Chair and Stephen P. Timoshenko Collegiate Professor of Mechanical Engineering
University of Michigan, Ann Arbor, MI 48109
(Previously Diefenderfer Chaired Professor in Mechanical Engineering at Penn State)

Charles E. Bakis
Distinguished Professor of Engineering Science and Mechanics
The Pennsylvania State University, University Park, PA 16802

Christopher D. Rahn
Professor of Mechanical Engineering
The Pennsylvania State University, University Park, PA 16802

Objectives

The objective of this investigation is to study the potential of utilizing fluidic flexible matrix composites (F^2MC) for autonomous structural tailoring. By taking advantages of the high anisotropy of flexible matrix composite (FMC) tubes and the high bulk modulus of the pressurizing fluid, significant changes in the effective modulus of elasticity could be achieved by controlling the inlet valve to the fluid filled F^2MC structure. The variable modulus F^2MC structure has the flexibility to easily deform when desired (open valve), possesses the high modulus required during loading conditions when deformation is not desired (closed valve – locked state), and has the adaptability to vary the modulus between the flexible/stiff states through control of the valve. In this investigation, we develop an accurate analytical modeling tool to predict the characteristics of a single F^2MC tube. Furthermore, we want to experimentally demonstrate at least an order of magnitude stiffness change in the F^2MC structure by valve control. Finally, as a first step to expand the concept of F^2MC tube and integrate it into complex structures, a test bed composed of a honeycomb-F^2MC sandwich structure variable transverse stiffness was conceived and built. We use analytical and experimental results to demonstrate the potential of this integrated structure.

REPORT DOCUMENTATION PAGE

Form Approved
OMB No. 0704-0188

PLEASE DO NOT RETURN YOUR FORM TO THE ABOVE ORGANIZATION.

1. REPORT DATE *(DD-MM-YYYY)*	2. REPORT TYPE	3. DATES COVERED *(From - To)*
08-09-2008	Final	October 1, 2006 – June 30, 2008

4. TITLE AND SUBTITLE
FLUIDIC FLEXIBLE MATRIX COMPOSITES FOR AUTONOMOUS STRUCTURAL TAILORING

5a. CONTRACT NUMBER
FA9550-07-1-0001

5b. GRANT NUMBER
FA9550-07-1-0001

5c. PROGRAM ELEMENT NUMBER

6. AUTHOR(S)
K. W. Wang
C. Bakis
C. Rahn

5d. PROJECT NUMBER

5e. TASK NUMBER

5f. WORK UNIT NUMBER

7. PERFORMING ORGANIZATION NAME(S) AND ADDRESS(ES)
The Pennsylvania State University
University Park, PA 16802

8. PERFORMING ORGANIZATION REPORT NUMBER

9. SPONSORING/MONITORING AGENCY NAME(S) AND ADDRESS(ES)
Air Force Office of Sponsored Research/NA
875 North Randolph Street, Suite 325, Room 3112, Arlington, Va., 22203-1768
Dr. Mitat Birkan

10. SPONSOR/MONITOR'S ACRONYM(S)
AFOSR

11. SPONSOR/MONITOR'S REPORT NUMBER(S)
AFRL-SR-AR-TR-08-0551

12. DISTRIBUTION/AVAILABILITY STATEMENT
Distribution A: Approved for Public Release

13. SUPPLEMENTARY NOTES

14. ABSTRACT

This project develops Fluidic Flexible Matrix Composites (F2MC) and structures that have controllable and reversible stiffness change. F2MC tubes are fiber wound and filled with fluid. If the fluid flows freely in and out of the tube then the stiffness is relatively low. Blocking the fluid flow by closing a valve results in high stiffness. In this investigation, we develop an accurate analytical model to predict and optimize F2MC tube performance and experimentally demonstrate 52 times stiffness change from open valve to closed valve. Tailoring the fiber wind angle and matrix material results in a broad range of open and closed valve stiffness values, indicating the wide applicability of the concept. Flexibility in the tube wall and air entrainment in the fluid are found to limit the maximum stiffness ratio that can be achieved. As a first step to develop variable stiffness structures, we model, design, build, and test a honeycomb-F2MC sandwich structure. This beam structure is cantilevered and demonstrates a three times increase in stiffness to an endpoint load from open valve to closed valve. The project demonstrates that F2MC technology has the potential to impact many applications, including soft robotics, isolation mounts, and morphing aircraft.

15. SUBJECT TERMS
Variable stiffness, modulus change, structures

16. SECURITY CLASSIFICATION OF:			17. LIMITATION OF ABSTRACT	18. NUMBER OF PAGES	19a. NAME OF RESPONSIBLE PERSON
a. REPORT	b. ABSTRACT	c. THIS PAGE		19	Kon-Well Wang
					19b. TELEPHONE NUMBER *(Include area code)* 734-764-2694

Status of Effort

In previous studies carried out by the PIs, a high mechanical advantage actuator system that is inspired by the fibrillar networks in plant cell walls was developed [1-3]. One of the basic elements in the actuator system is a composite tube consisting of a flexible matrix and multiple layers of oriented, high performance fibers such as carbon (See Fig. 1). By tailoring the properties of the fibers and matrix of the flexible matrix composite (FMC) tube, one can create a material that is flexible in certain directions yet compliant in others. For example, the ratio of Young's moduli in the directions parallel and transverse to the fibers can range from 10^2 to 10^4. Strands of such FMC material can be wound into a tube at selected angles relative to the winding axis (a process called filament winding) such that the tube can contract or elongate axially via internal pressurization. It was previously shown that large strain and large force can be achieved with individual, pressurized FMC tubes [1-3] and that parallel arrays of tubular elements can be integrated to form 2-dimensional adaptive structures (e.g., skins and plates with multiple tubes) [1].

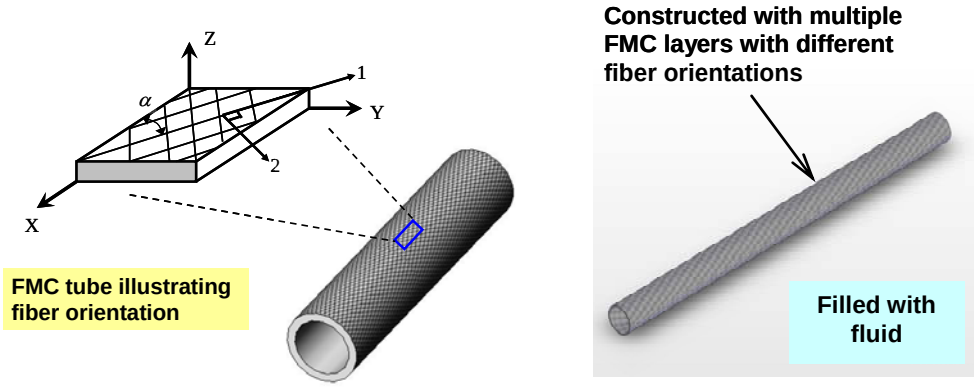

Fig. 1. Flexible matrix composite tube illustrating fiber orientation (left) and F^2MC tube with multiple FMC layers and filled with fluid (right).

Building upon and expanding from the previous research experience [1-3], the new idea proposed in this project is to synthesize an adaptive structure with variable mechanical properties utilizing fluidic FMC (F^2MC) tube elements, through valve control. By using high bulk modulus working fluids in conjunction with FMC tubes having selective fiber orientations, one can obtain significant changes in stiffness by simply opening or closing an inlet valve to the F^2MC tubes (Fig. 2). With an open valve, the system can be very flexible. Due to its high bulk modulus, the fluid is highly resistant to volume change when the valve is closed. Because of the fiber reinforcement, the fluid-filled FMC tubes will thus develop very high stiffness. The variable stiffness tube has the flexibility to be easily deformed when desired (low stiffness with open valve and circulating fluid) and to sustain significant loads when deformation is not desired (high stiffness with closed valve and no circulation). These interesting capabilities of single F^2MC tubes can also be carried over to multi-cellular structures composing many small-diameter F^2MC tubes integrated into supporting matrix materials. The wide range of change in stiffness is valuable in many existing and potential applications, such as soft robotics, isolation mounts, and morphing aircraft.

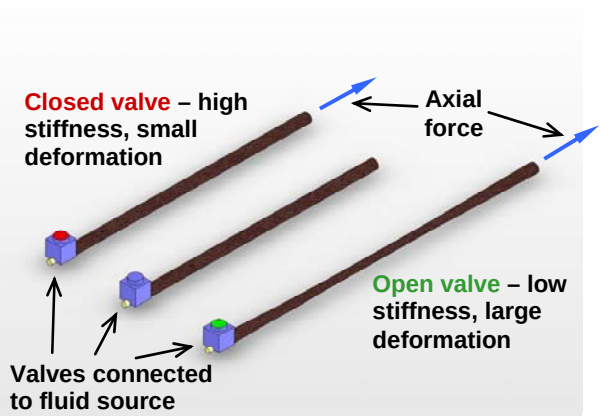

Fig. 2. Variable stiffness F^{2}MC tube.

In a previous effort by the authors [4], a simple model of the fluid-filled F^{2}MC composite single tube was developed using a composite thin shell theory. The results from the model predicted that more than two orders of magnitude change in the stiffness of the F^{2}MC tubes could be achieved between the open and closed valve configurations. However, there are several limitations to the model. First, the model does not consider the effect of a thin inner lining layer between the fluid and the FMC laminate. The inner lining layer may be needed to prevent leakage due to the high internal pressure generated by axial loading in the closed valve condition. Second, thin shell theory does not take into account the radial compliance of the FMC wall. Finally, the previous model does not take into account the possibility of air entrainment in the working fluid. Such issues should be accounted for to accurately predict the stiffness of the tube—particularly in the closed valve configuration where all sources of compliance are important.

Accomplishments/New Findings

In the new reporting period, we have developed a more comprehensive model that can better capture the open/closed valve characteristics of the F^{2}MC single tube system. The F^{2}MC single tube is modeled as a structure composed of two concentric cylinders filled with a compressible fluid: an inner liner layer and an outer FMC laminate as shown in Fig. 3.

As can be seen from Fig. 3, an elastomeric inner liner is subjected to a pressure p_1 at the inner surface and a pressure of p_2 at the outer surface. Therefore, we have the following equations for the inner liner [5]

$$\sigma_r^{(i)} = \frac{p_1 a_0^2 - p_2 a_1^2}{a_1^2 - a_0^2} - \frac{a_1^2 a_0^2}{r^2 (a_1^2 - a_0^2)}(p_1 - p_2) \tag{1}$$

$$\sigma_\theta^{(i)} = \frac{p_1 a_0^2 - p_2 a_1^2}{a_1^2 - a_0^2} + \frac{a_1^2 a_0^2}{r^2 (a_1^2 - a_0^2)}(p_1 - p_2) \tag{2}$$

$$\sigma_z^{(i)} = \frac{F_1}{\pi (a_1^2 - a_0^2)} \tag{3}$$

$$\varepsilon_r^{(i)} = \frac{1}{E}\left[\sigma_r^{(i)} - \nu\left(\sigma_\theta^{(i)} + \sigma_z^{(i)}\right)\right] \tag{4}$$

$$\varepsilon_\theta^{(i)} = \frac{1}{E}\left[\sigma_\theta^{(i)} - \nu\left(\sigma_r^{(i)} + \sigma_z^{(i)}\right)\right] \tag{5}$$

$$\varepsilon_z^{(i)} = \frac{1}{E}\left[\sigma_z^{(i)} - \nu\left(\sigma_r^{(i)} + \sigma_\theta^{(i)}\right)\right] \tag{6}$$

where F_1 is the resultant of the axial stress, $\sigma_z^{(i)}$, over the cross-sectional area of the inner liner.

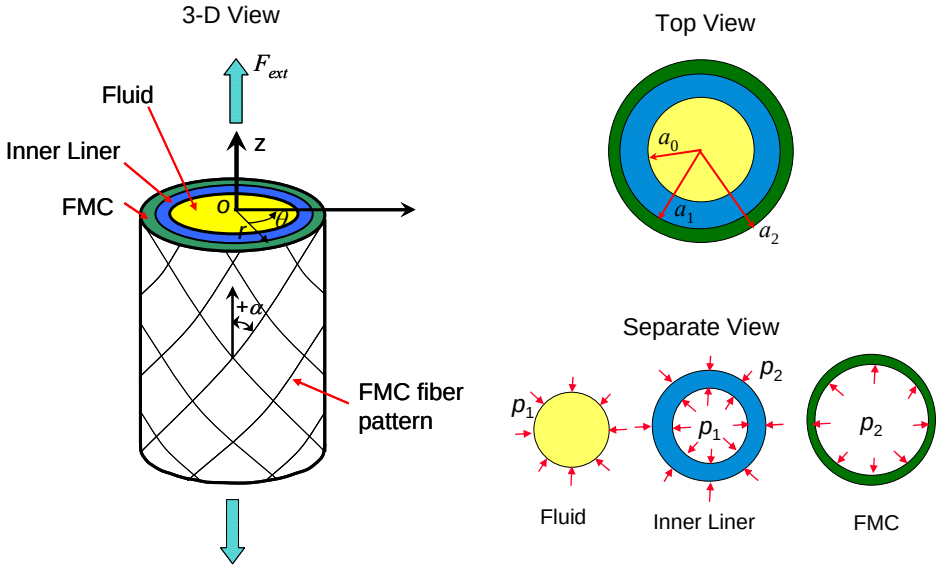

Fig. 3. Illustration of an F^{2}MC tube structure.

The outer FMC laminate is subjected to a pressure of p_2 at the inner surface as shown in Fig. 3. Therefore, Lekhnitskii's elasticity solution for a homogenous orthotropic cylinder under an axial load and an internal pressure is used to model the FMC laminate [6]. According to Lekhnitskii, the stress/strain components in a homogeneous orthotropic FMC tube can be determined from the following equations

$$\sigma_r^{(o)} = \frac{p_2 c_2^{k+1}}{1-c_2^{2k}}\rho^{k-1} + \frac{-p_2}{1-c_2^{2k}}c_2^{k+1}\rho^{-k-1} + \frac{\varepsilon_z^0}{a_{33}}h\left(1 - \frac{1-c_2^{k+1}}{1-c_2^{2k}}\rho^{k-1} - \frac{1-c_2^{k-1}}{1-c_2^{2k}}c_2^{k+1}\rho^{-k-1}\right) \tag{7}$$

$$\sigma_\theta^{(o)} = \frac{p_2 c_2^{k+1}}{1-c_2^{2k}}k\rho^{k-1} + \frac{-p_2}{1-c_2^{2k}}kc_2^{k+1}\rho^{-k-1} + \frac{\varepsilon_z^0}{a_{33}}h\left(1 - \frac{1-c_2^{k+1}}{1-c_2^{2k}}k\rho^{k-1} + \frac{1-c_2^{k-1}}{1-c_2^{2k}}kc_2^{k+1}\rho^{-k-1}\right) \tag{8}$$

$$\sigma_z^{(o)} = \frac{\varepsilon_z^0}{a_{33}} - \frac{1}{a_{33}}\left(a_{13}\sigma_r^{(o)} + a_{23}\sigma_\theta^{(o)}\right) \tag{9}$$

$$\varepsilon_r^{(o)} = a_{11}\sigma_r^{(o)} + a_{12}\sigma_\theta^{(o)} + a_{13}\sigma_z^{(o)} \tag{10}$$

$$\varepsilon_\theta^{(o)} = a_{12}\sigma_r^{(o)} + a_{22}\sigma_\theta^{(o)} + a_{23}\sigma_z^{(o)} \tag{11}$$

$$\varepsilon_z^{(o)} = a_{13}\sigma_r^{(o)} + a_{23}\sigma_\theta^{(o)} + a_{33}\sigma_z^{(o)} \tag{12}$$

where $c_2 = \frac{a_1}{a_2}$, $\rho = \frac{r}{a_2}$, a_{ij} are the effective 3-dimensional elastic compliance constants of the FMC laminate in the cylindrical coordinate system, and *k* and *h* are determined from the following equations [6]

$$k = \sqrt{\frac{\beta_{11}}{\beta_{22}}} \tag{13}$$

$$h = \frac{a_{23} - a_{13}}{\beta_{11} - \beta_{22}} \tag{14}$$

where $\beta_{11} = a_{11} - \frac{a_{13}^2}{a_{33}}$ and $\beta_{22} = a_{22} - \frac{a_{23}^2}{a_{33}}$. As can be seen from Eqs. 10-12, Lekhnitskii's model requires the 3-dimensional elastic properties of the laminate. The thick laminate analysis by Sun and Li [7] is used to generate the effective 3-dimensional elastic constants of the laminate from lamina properties. The overall inputs to the F^{2}MC model are the inner liner material properties (E, ν), the FMC laminate fiber angles ($\pm\alpha$), and FMC lamina properties. Since the FMC lamina is assumed to be transversely isotropic, only E_1, E_2, G_{12}, ν_{12}, and ν_{23} are needed for the inputs.

For representing the closed valve scenario, it is assumed that the tube is filled and sealed at zero pressure with a volume V_0 of compressible fluid of bulk modulus B. With the application of F_{ext}, the enclosed volume of the tube is changed by the amount ΔV. Corresponding to this volume change, the pressure of the fluid changes from zero to p_1 and can be expressed using the following relationship

$$B\left(\frac{\Delta V}{V_0}\right) = -p_1 \,. \tag{15}$$

Expressing the volume change in terms of tube strains and neglecting the higher order terms, Eq. 15 can be simplified to

$$B\left(\varepsilon_z^{(i)}\Big|_{r=a_0} + 2\,\varepsilon_\theta^{(i)}\Big|_{r=a_0}\right) = -p_1 \,. \tag{16}$$

Equations 1-16 can be solved with the following equilibrium and compatibility equations. It is assumed that the entire F^{2}MC tube is stretched uniformly with an axial strain of ε_z^0, therefore

$$\varepsilon_z^{(i)} = \varepsilon_z^{(o)} = \varepsilon_z^0 \,. \tag{17}$$

At the inner liner/FMC interface, the radial displacement has to be continuous,

$$u_r^{(i)}\Big|_{r=a_1} = u_r^{(o)}\Big|_{r=a_1} \tag{18}$$

which can also be expressed in terms of hoop strain as

$$\varepsilon_\theta^{(i)}\Big|_{r=a_1} = \varepsilon_\theta^{(o)}\Big|_{r=a_1} \,. \tag{19}$$

At each end of the F^{2}MC tube, we have the following equilibrium equation

$$F_1 + F_2 = F_{ext} + p_1 \pi a_0^2 \tag{20}$$

where F_2 is the is the resultant of the axial stress distributed over the cross-sectional area of the FMC laminate, $\sigma_z^{(o)}$, and can be determined as

$$\frac{F_2}{2\pi} = \int_{a_1}^{a_2} \sigma_z^{(o)} r dr \,. \tag{21}$$

The effective closed valve modulus of the F^{2}MC tube is defined as

$$E_{closed} = \frac{F_{ext}}{\pi a_2^2} \,. \tag{22}$$

For the open valve case, p_1=0. Therefore, one can simply assign B=0 in the above solving process to calculate E_{open}. The closed/open modulus ratio, R, is defined as

$$R = \frac{E_{closed}}{E_{open}} \,. \tag{23}$$

We conducted a number of experiments to validate the new model. The F^{2}MC tubes were wet filament wound using a McClean-Anderson filament winding machine. Tensile tests of F^{2}MC tubes were performed on a 13 kN (3 kip) axial servo-hydraulic load frame (MTS 810) as shown in Fig. 4 For all tests, a load rate of 0.2 mm/s (0.008 in/s) in tension was used. An Ashcroft pressure transducer (Model # K17M0215F22000) with a 13.8 MPa (2000 psi) pressure capability provided high resolution measurements during loading. Manual ball valves with a 13.8 MPa (2000 psi) pressure rating were used for the open- and closed-valve scenarios.

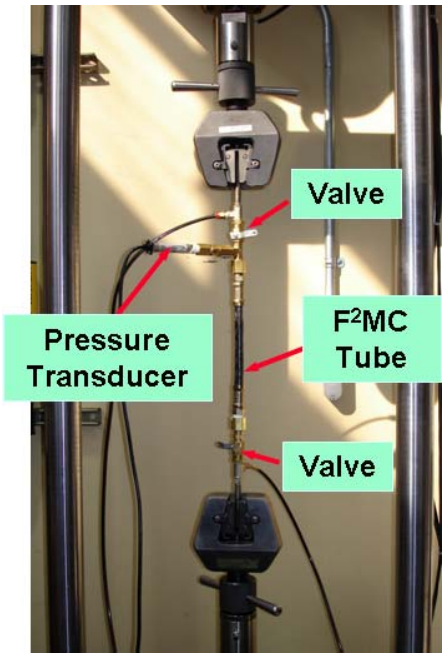

Fig. 4. Tensile test setup for a single F^{2}MC tube.

A parametric study was performed using the proposed model. The parameters shown in Table 1 are used as the baseline parameters. For easy comparison, during the analysis, only one parameter is varied at a time, and all other parameters are kept the same as the baseline.

Table 1. Baseline parameters used in the model analysis.

	Property	Value
FMC Lamina	E_1	115 GPa
	E_2	1.8 MPa
	G_{12}	1.4 MPa
	ν_{12}	0.33
	ν_{23}	0.93
Inner Liner	E	0.1 GPa
	ν	0.497
Geometry	a_0	5 mm
	a_1	6 mm
	a_2	6.5 mm
Fluid	B	2.0 GPa
	α_A^0	0

The effect of fluid bulk modulus on the modulus ratio of F^{2}MC tubes is shown in Fig. 5. The working fluid inside the F^{2}MC tube performs a vital role. The constraining action of the fibers and the high bulk modulus of the working fluid provide the increased modulus of the closed valve condition over the open valve condition. One would expect a fluid of larger bulk modulus to lead to a larger modulus ratio. However, it is seen in Fig. 5 that a change in fluid bulk modulus from B=0.1 to 10 GPa introduces only very little change in modulus ratio. This can be explained by examining the difference in bulk modulus between the working fluid and the inner liner material. For example, water has a bulk modulus of about 2 GPa, whereas, the bulk modulus of the inner liner calculated using parameters given in Table 1 has a value of only 5.6 MPa ($K = E/3(1-2\nu)$)—i.e., more than 2 orders of magnitude less than that of water. Thus, under a closed valve condition, the compliant inner liner is compressed much more than the water, preventing the full utilization of the working fluid.

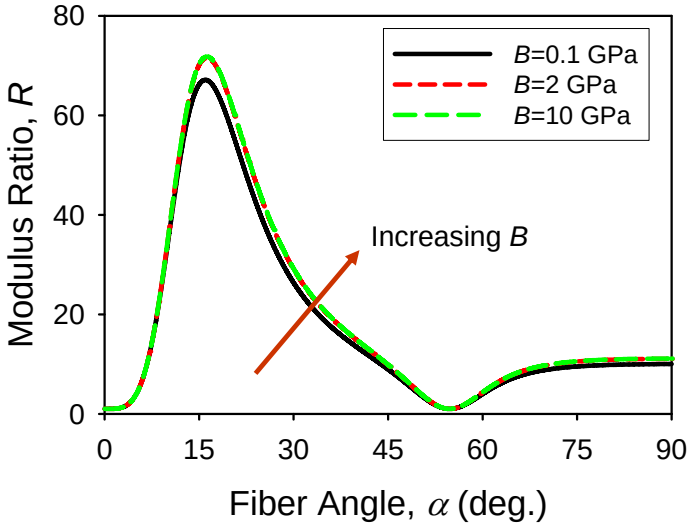

Fig. 5. Effect of fluid bulk modulus, B, on the modulus ratio of F^{2}MC tubes of fiber angle $\pm\alpha$.

To better illustrate the effects of the inner liner characteristics on the overall modulus ratio, the liner modulus and thickness are varied from the baseline in Figs. 6 and 7, respectively. As can be seen from Fig. 6, the maximum achievable modulus ratio changes from 70 at E=0.1 MPa, to

~120 at E=1 MPa, and then decreases to ~65 at E=10 MPa. To a certain limit, increasing the inner liner modulus will make the inner liner more difficult to compress under closed valve conditions, thus generating high internal pressure. As a consequence, a high closed/open valve modulus ratio can be achieved. However, an excessive increase in inner liner modulus results in a higher open valve modulus, causing the closed/open modulus ratio to decrease. Figure 7 shows that the inner liner modulus of elasticity and the fiber angle can be tailored so that a maximum modulus ratio can be achieved. As can be seen from Fig. 7, the effect of the inner liner thickness on the modulus ratio is quite simple: thinner liners result in higher modulus ratios. As mentioned previously, compared to the working fluid, the inner liner material is much more compressible. Therefore, reducing the inner liner thickness results in less liner volume reduction under high internal pressure. As a result, the overall closed valve modulus and modulus ratio of the F^{2}MC tube are increased. From Fig. 7, it can be seen that the best modulus ratio is achieved without an inner liner. However, in practical situations, it may be difficult to withstand a large internal pressure without at least a thin inner liner.

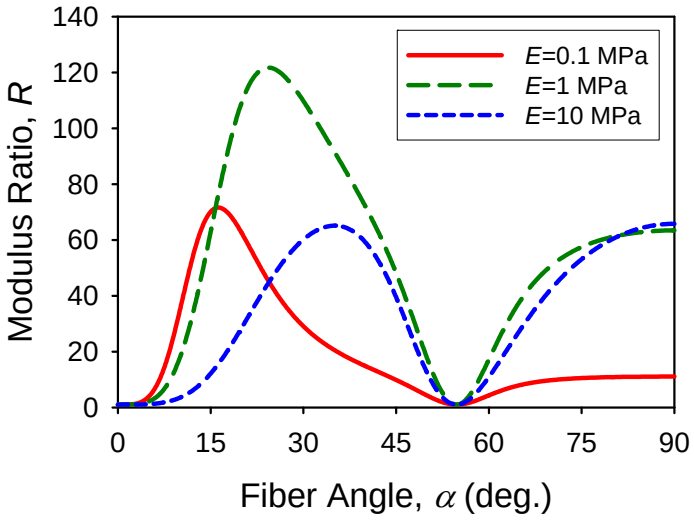

Fig. 6. Effect of inner liner modulus, E, on the modulus ratio of F^{2}MC tubes of fiber angle $\pm\alpha$.

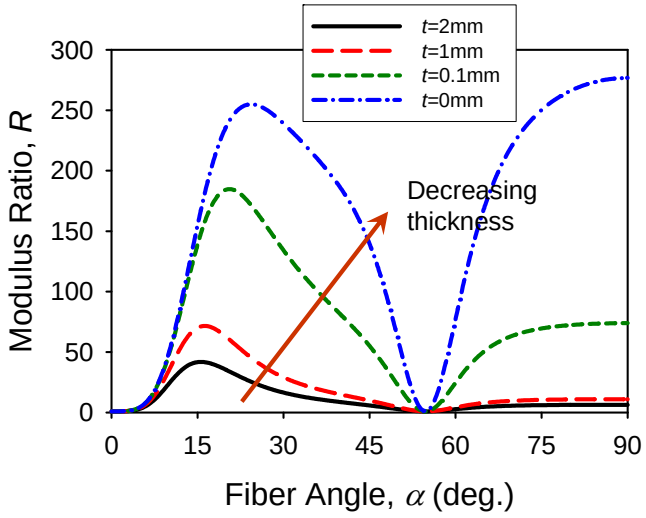

Fig. 7. Effect of inner liner thickness, t (=a_1-a_0), on the modulus ratio of F^{2}MC tubes of fiber angle $\pm\alpha$.

For the purpose of model validation, F^{2}MC tubes with inner liners of two different moduli are fabricated. The lower modulus inner liner material of the two is made of Dragon Skin® silicone (Smooth-On Inc., Easton, PA) (E=0.09 MPa, ν=0.497), and the higher modulus inner is made of QSil® 270 (Quantum Silicones Inc., Richmond, VA) (E=8.2 MPa, ν=0.495). The baseline F^{2}MC tube geometries and FMC lamina properties are the same as in Table 1. Experimentally measured open-valve and closed-valve moduli and modulus ratios for various tube configurations are summarized in Table 2. Typical measured open- and closed-valve stress-strain curves of an F^{2}MC tube are shown in Fig. 8. As can be seen from the figure, the stress-strain curve for the closed-valve condition shows a two-staged behavior: a nonlinear initial portion, followed by a linear portion. The initial nonlinear behavior is due to the air entrapment in the system. The closed-valve modulus is determined by calculating the slope of the linear portion of the closed-valve stress-strain curve. For the case shown in Fig. 8, a modulus ratio of 56 is achieved. It can also be noticed from Fig. 8 that the internal pressure increases linearly with the applied external load. A maximum internal pressure of 10 MPa (~1500 psi) is recorded with an applied axial stress of 35 MPa.

Table 2. F^{2}MC tubes fabricated for tension testing.

Sample #	Liner Layer Material	FMC Laminate Material	E_{open}	E_{closed}	R
A	Silicone: QSil 270	±35-deg. carbon fiber with silicone matrix (Dragon Skin)	27 MPa	1.5 GPa	56
B	Silicone: QSil 270	±45-deg. carbon fiber with silicone matrix (Dragon Skin)	12 MPa	0.35 GPa	29
C	Silicone: QSil 270	±55-deg. carbon fiber with silicone matrix (Dragon Skin)	3.2 MPa	4.8 MPa	1.5
D	Silicone: Dragon Skin	±35-deg. carbon fiber with matrix silicone matrix (Dragon Skin)	4.6 MPa	0.11 GPa	24

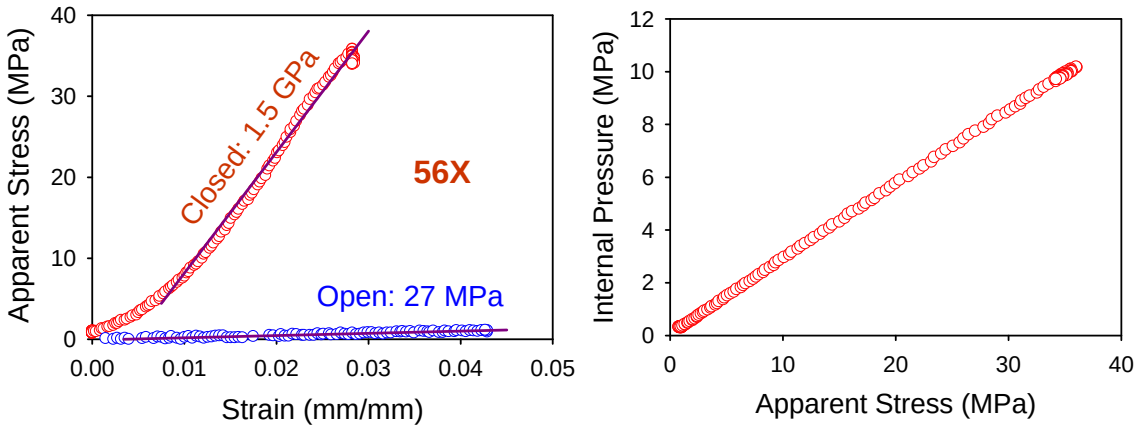

Fig. 8. Experimental results of a ±35-deg. F^{2}MC tube with stiff inner liner: (left) applied stress vs. strain curve; (right) internal pressure vs. applied stress curve.

A comparison between predicted and experimentally measured modulus ratios and closed valve moduli for F^{2}MC tubes with soft and stiff inner liners are shown in Fig. 9. The model shows reasonable agreement with experimental data. Also, the experimental results confirm the prediction that using a higher elastic modulus inner liner results in a higher closed-valve modulus.

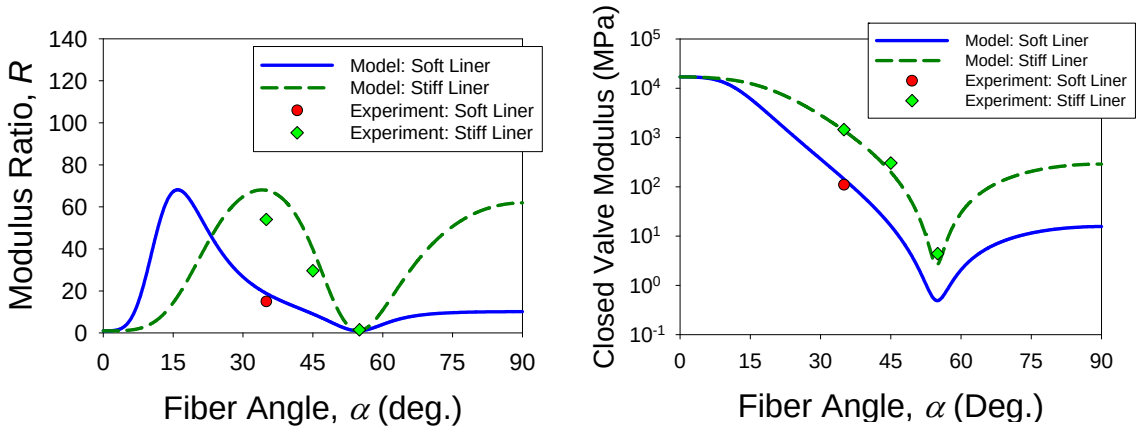

Fig. 9. Comparison between model prediction and experimental data for $\pm\alpha$ F^{2}MC tubes with soft and stiff inner liners: (left) modulus ratios; (right) closed-valve modulus.

Based on the preliminary validation of the new model shown above, it is possible to perform a study of the design space for F^{2}MC structures. One advantage of the F^{2}MC technology is that one can tailor the material properties for different applications. For example, we can vary some of the FMC lamina properties (E_1, E_2, G_{12}, α) and inner liner material properties (E) as well as the F^{2}MC tube geometry (a_0, a_1, a_2) for illustrative purposes. Table 3 lists the controlling parameters in the design space study and their feasible ranges, whereas all other parameters are kept the same as in Table 1. In order to populate the possible design space, each parameter is randomly selected from within the ranges shown in Table 3. These randomly picked parameters are then used as inputs to the model to calculate the open- and closed-valve moduli and the modulus ratio of the F^{2}MC tube. In the current study, a total of 20,000 randomly picked configurations were calculated to obtain a clear picture of the design space. The resulting open valve moduli (indicated on the plot as "lower modulus") versus modulus ratios are plotted as individual points in Fig. 10. As can be seen, the data points from this limited study occupy almost the entire lower-left triangular area on the plot, indicating an extraordinarily wide range of possible properties attainable with F^{2}MC technology. Several existing variable modulus materials, such as shape memory alloy (SMA) [8,9], shape memory polymer (SMP) [10,11], piezoelectric ceramic (PZT) [12], piezoelectric single crystal (PZN-PT) [13], magnetostrictive material using Terfenol-D [14], electrochemo-mechanical conducting polymer [15], ionic gel [12], magneto-rheological (MR) elastomer [16,17], dielectric polymers using polyvinylidene fluoride (PVDF) [12], etc. are also plotted in Fig. 10 for comparison. Compared to the other materials, the F^{2}MC concept has many advantages: a much wider range of tailorablity; a passive characteristic not requiring significant external power (electricity, magnetic field, temperature, etc.) to switch or maintain different states of modulus; and a very fast response time (only limited by the switching speed of the valve being used).

Table 3. F^{2}MC parameter ranges for the design space study.

Variable	Range	Description
E_1	20 ~ 200 GPa	FMC lamina fiber direction modulus
E_2	1 ~ 1000 MPa	FMC lamina transverse direction modulus
E	0.1 ~ 1000 MPa	Inner liner modulus
α	0 ~ 90 deg.	FMC laminate fiber angle
r_1	0 ~ (1-r_2)	Inner liner thickness ratio: $r_1=(a_1-a_0)/a_2$
r_2	0.00005 ~ 0.5	FMC laminate thickness ratio: $r_2=(a_2-a_1)/a_2$

*Lamina property G_{12} is assumed to be $0.75 \cdot E_{22}$.

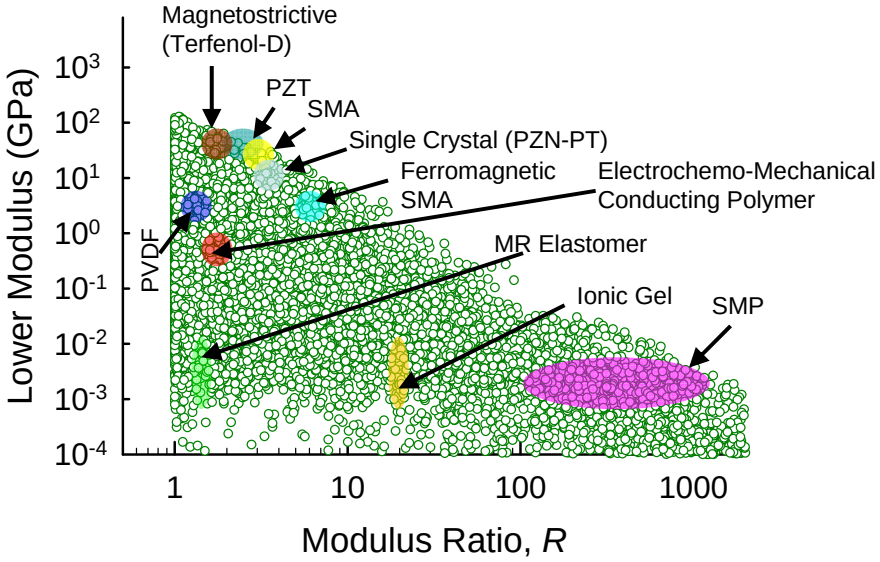

Fig. 10. Design space of F^{2}MC tubes and other variable modulus materials (open circles indicate feasible designs).

To further expand the concept of F^{2}MC tube, a variable transverse stiffness honeycomb panel is proposed in this study, where the traditional aluminum or laminated composite face sheets are replaced by layers of F^{2}MC tubes embedded in a soft matrix material (Fig. 11). A honeycomb core is effective in transferring the transverse load on the sandwich panel into axial loads on F^{2}MC tubes, so that the variable F^{2}MC stiffness in its axial direction is transformed into variable panel stiffness in its transverse direction. The concept of tube segmentation is introduced to further increase the variable stiffness ratio; it can be realized by an embedded valve network.

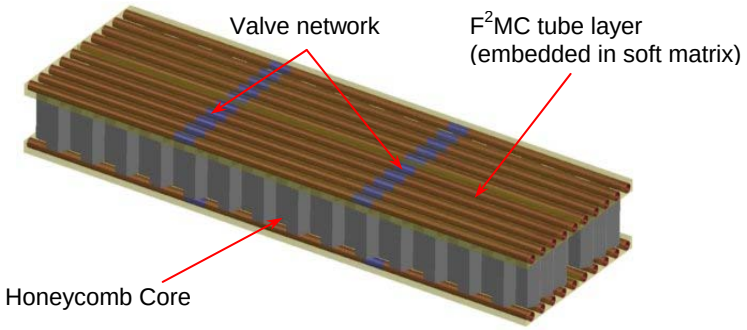

Figure 11. A sandwich panel using segmented F^{2}MC for variable bending stiffness.

Figure 12 shows a schematic of a sandwich beam subject to a transverse end load *F*, and end moment *M*. Only one F^{2}MC tube is applied at the top to simplify the analysis and test. A thin center sheet made of spring steel (much stiffer than the F^{2}MC tube) constitutes the neutral axis in both the open and closed valve scenarios.

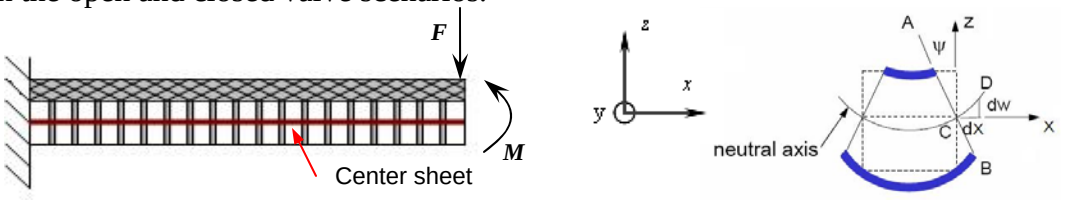

Figure 12. Schematic diagram of the sandwich beam and the assumed displacement field.

The Lekhnitskii's solution used in previous study is combined with Timoshenko shear-deformable beam theory to study the elastic behavior of the sandwich structure. With these two theories, we derived the total elastic energy of the beam in an explicit form and therefore obtained a closed-form solution for the beam deformation by applying variational calculus.

Based on the Timoshenko beam theory, the displacement-strain relationships of the honeycomb core and F^{2}MC tube can be described in Eqs. (24, 25) [18],

$$\varepsilon_x(x) = -z\frac{d\psi(x)}{dx}, \tag{24}$$

$$\varepsilon_{xz}(x) = \frac{1}{2}\left[\frac{dw(x)}{dx} - \psi(x)\right], \tag{25}$$

where *w(x)* is the vertical deflection of the neutral axis, and $\psi(x)$ is the angular rotation of the vertical cross section plane (See Fig. 12), ε_x and ε_{xz} are the longitudinal normal strain and tensor shear strain of the beam, respectively.

The Lekhnitskii's solution is applied to analyze the stress and strain distribution of the laminated F^{2}MC tube. The stress and strain of inner liner can be described based on equations 1, 2, and 4-6, and those of fiber matrix tube wall can be described based on equations 7-14.

Three compatibility conditions are necessary to guarantee and consistency between Timoshenko beam theory and Lekhnitskii's solution. The first compatibility condition is that the average axial strains in the inner and outer tube layers from Lekhnitskii's solution (Eq. 6, 12) agree with the strain field of the Timoshenko beam model (Eqs. 24) at the center of the tube,

$$\varepsilon_x^{(o)} = \varepsilon_x^{(i)} = -h_o\frac{d\psi}{dx}, \tag{26}$$

where h_o is the distance between the center axis of the F^{2}MC tube and the center sheet of the beam. The second compatibility condition is the strain continuity at the interface of F^{2}MC inner liner and fiber composite tube wall (Eqs. 19).

The first two compatibility conditions apply for both open and closed valve scenarios. While the valves are closed, in particular, a third compatibility conditions is necessary to correlate the tube deformation to working fluid pressure.

$$p_1 = -B\frac{\Delta V}{V} = -B\frac{\int_0^L [2\varepsilon_\theta^{(i)}|_{r=a_o} + \varepsilon_x^{(i)}|_{r=a_o}]dx}{L}. \tag{27}$$

where L is the beam length, B is the fluid bulk modulus, this is a more general formulation compared to Eqs. 16.

We obtained the elastic energy of the F^{2}MC tube from its normal stress and strain for the assumed deformation field by integrating the inner product of the stress and strain vectors over the defined volume,

$$\Pi_{F^2MC,normal} = \frac{1}{2}\int_0^L\int_0^{2\pi}\int_{a_1}^{a_2}\{\varepsilon^{(o)}\}^T\{\sigma^{(o)}\}rdrd\theta dx + \int_0^L\int_0^{2\pi}\int_{a_0}^{a_1}\{\varepsilon^{(i)}\}^T\{\sigma^{(i)}\}rdrd\theta dx = \frac{1}{2}H_p(\psi|_0^L)^2 + \frac{1}{2}H_b\int_0^L(\frac{d\psi}{dx})^2dx\,, \tag{28}$$

where H_p and H_b are constants derived from the material properties appearing in appearing in the formulation of Lekhnitskii's solution

The honeycomb core is modeled as a homogeneous material with anisotropic shear and bending modulus. When the control valves are closed, the total potential energy of the honeycomb-F^{2}MC sandwich beam for the assumed deformation field is obtained by

$$\Pi_{total} = \frac{1}{2}[\sum_{n=1}^{2}(EI)_n + H_b]\int_0^L(\frac{d\psi}{dx})^2dx + \frac{1}{2}[H_p + \frac{V_o}{2B}H_p^2](\psi|_0^L)^2 + \frac{1}{2}\sum_{m=1}^{4}(kGA)_m\int_0^L(\frac{dw}{dx}-\psi)^2dx - Fw|_L - M\psi|_L \tag{29}$$

where the subscripts $_n$ and $_m$ denote the different beam components with 1 referring to honeycomb, 2 to center sheet, 3 to inner liner and 4 to fiber composite wall. EI is the bending stiffness of the corresponding component, G is the axial shear modulus including the F^{2}MC tube, A is the corresponding cross-section area, and k is the shear coefficient. V_o is the initial working fluid volume and B is the fluid bulk modulus. F and M denote the external load and moment applied at the free end of the cantilever beam (Fig. 12).

Applying variational calculus, the deformation of the beam is written explicitly as

$$\psi(x) = \frac{(2D_{EI}+D_P)Lx - (D_{EI}+D_P)x^2}{2(D_{EI}+D_P)D_{EI}}F\,, \tag{30}$$

$$w(x) = \frac{x}{G}F + \frac{(6D_{EI} + 3D_P)Lx^2 - (2D_{EI} + 2D_P)x^3}{12(D_{EI} + D_P)D_{EI}}F \tag{31}$$

For simplicity, we denote G (= $\sum kGA)_m$) as the net *shear modulus* from the sandwich beam components; D_{EI} (= $\sum(EI)_n + H_b$) as the net *bending stiffness* from material elasticity. D_P (= $(H_p+V_oH_p^2/2B)L$) is the extra load resistance from closing the valve, denoted the *pressure-induced stiffness*.

The equivalent *transverse stiffness* of the beam is obtained by dividing the magnitude of external load by the transverse beam deflection at the point of the applied load. When the valve is closed, this stiffness ($\hat{E}_C$) is obtained as follows

$$\hat{E}_C = \frac{F}{w(x=L)} = \frac{1}{\frac{L}{G} + \frac{4D_{EI} + D_P}{12D_{EI}(D_{EI} + D_P)}L^3}. \tag{32}$$

When the valves are open, the beam transverse stiffness ($\hat{E}_O$) is obtained from equation 31 by setting the pressure-induced stiffness to zero. Finally, the *transverse stiffness ratio* between closed and open valve scenarios is defined as follows,

$$R = \frac{\hat{E}_C}{\hat{E}_O} = \frac{w_O(x=L)}{w_C(x=L)} = \frac{\frac{1}{G} + \frac{L^2}{3D_{EI}}}{\frac{1}{G} + \frac{(4D_{EI} + D_P)L^2}{12D_{EI}(D_{EI} + D_P)}}, \tag{33}$$

Load-deflection test was performed on a beam prototype with one single-segment F^2MC tube to verify the analytical results (Fig. 13). The honeycomb layer was fabricated by attaching two aluminum honeycomb strips onto a spring steel strip using all-purpose epoxy. To avoid any interlayer slip between the F^2MC tube and aluminum honeycomb, a cylindrical shaped groove was machined on the honeycomb to cradle the F^2MC tube. The tube was bonded to this groove with epoxy. Custom fittings were made to connect the tube, the miniature ball valves and the pressure gauge (PX309-050A5V, Omegadyne Inc. Sunbury, OH). The test specimen was cast in urethane rubber (Reo-flex 20, Smooth-On Inc. A rectangular grid pattern was applied to the rubber surface to assist in measuring the beam deformation (Fig. 13, right).

The honeycomb sandwich beam provides good versatility as a wide range of design parameter combinations can be selected. Tables 4 and 5 summarize the selection of design parameters used for the baseline study. As implied by equations 30-31, these design parameters can be formulated into three factors: net shear modulus (G), net bending stiffness (D_{EI}), and pressure-induced stiffness (D_P). The magnitude and characteristics of the beam transverse deflection are dominated by these three factors.

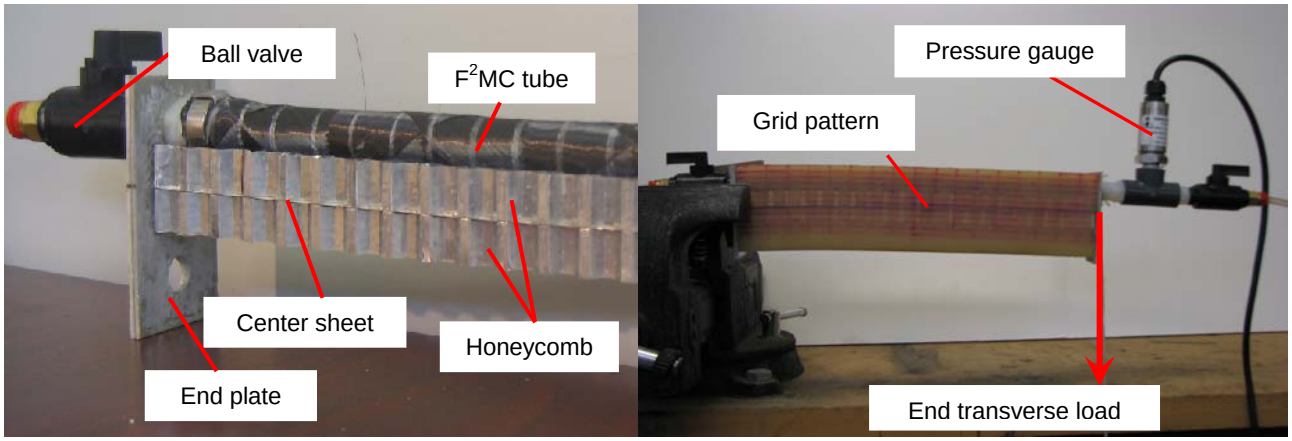

Figure 13. Honeycomb sandwich specimen before being cast in rubber (left); and experiment setup, showing grid pattern (right).

Table 4. Material properties and design factors used for baseline study and prototype fabrication.

	Property	Value		Property	Value
F^2MC ($\pm 35^o$)	Fiber composite shear modulus (G)[6]	0.84 MPa	Geometry Design	Fiber composite outer radius (a_2)	7.5 mm
	Fiber composite shear coef. (k)	0.62[9]		Fiber composite inner radius (a_1)	6.5 mm
	Inner liner modulus (E)	8.2 MPa		Inner liner inner radius (a_0)	5.5 mm
	Inner liner Poisson's ratio (v)	0.495		Honeycomb cross-section (A)	5.1 cm^2
	Inner liner shear modulus (G)	2.74 MPa		Center sheet cross-section (A)	3.2 mm^2
	Inner liner shear coef. (k)	0.62[9]		Fiber composite cross-section (A)	43.96 mm^2
Honey-comb	Shear modulus (G)	640 MPa		Inner liner cross-section (A)	37.68 mm^2
	Shear coef. (k)	0.43[10, 11]		Beam length (L)	25 cm
	Bending stiffness (EI)	0.40 Nm^2	Center Sheet	Shear modulus (G)	27 GPa
Fluid	Bulk modulus (B)	2 GPa		Shear coef. (k)	0.86[9]
Pressure factors	K_1 (Eq. 12)	-35.7 MPa/rad		Bending stiffness (EI)	9.5x10^{-4} Nm^2
	K_2 (Eq. 13)	-35.4 MPa/rad	Net Stiffness	Net bending stiffness (D_{EI})	2.0 Nm^2
	K_3 (Eq. 13)	-61.4 kPa*m/rad		Pressure-induced stiffness (D_P)	274 Nm^2

Table 5. Components of the compliance matrix of the fiber composite used for baseline study (Eqs. 9 – 12.)

a_{11}	0.145 MPa^{-1}	a_{12}	-0.148 MPa^{-1}	a_{13}	0.072 MPa^{-1}
a_{22}	0.311 MPa^{-1}	a_{23}	-0.153 MPa^{-1}	a_{33}	0.075 MPa^{-1}

Figure 14 demonstrates the deformation of a cantilever sandwich beam under an end point transverse load. When the valves are open, the transverse beam deflection equals that of a classical Timoshenko beam. When the valves are closed, the extra pressure-induced stiffness causes the beam to deform into an "S" shape, where both transverse deflection w and cross-section angular rotation ψ at the free end are reduced (See the solid line in Fig. 14). One can obtain the smallest possible beam transverse deflection in the closed valve scenario by setting the shear modulus (G) and pressure-induced modulus (D_P) to infinity (Fig. 14, dashed line). Then the beam behaves as if its free end angular rotation is restricted. The highest possible transverse stiffness ratio for a sandwich beam with single-segment F^2MC tube is obtained similarly by setting G and D_P to infinity in equation 33. This maximum ratio is 4 regardless of the magnitude of bending stiffness (D_{EI}).

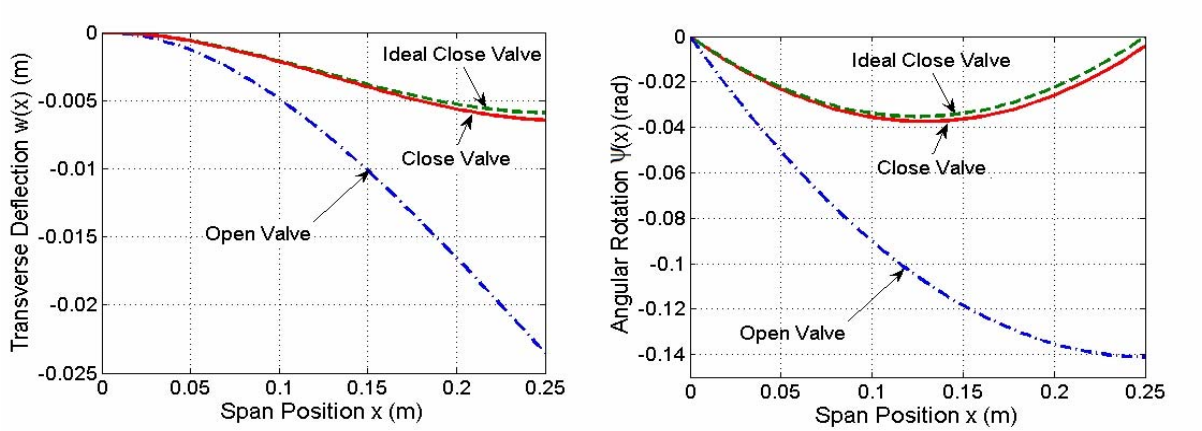

Figure 14. Transverse beam deflection in closed valve scenario of baseline study and its best possible performance. Beam made of ±35° F²MC tube, 2 cm honeycomb core.

A parametric study is carried out to derive guidelines for the design of F²MC tubes for a high degree of influence on beam bending stiffness. The three studied design parameters of F²MC tube are its carbon fiber orientation, inner liner stiffness, and inner liner thickness. While the honeycomb specifications are kept constant as in Table 4, Fig. 15 summarizes the study results. The F²MC tubes give better transverse stiffness ratio at different fiber angles, depending on the properties of inner liner. The inner liner, although necessary for sealing the tube, has a negative effect on providing variable stiffness ratio. For a given inner liner modulus, the thicker the liner, the smaller the beam transverse stiffness ratio becomes. The modulus of the inner liner, on the other hand, can limit the fiber angle range where the stiffness ratio is maximized. For the study presented in Fig. 15, 1 to 10 MPa is the optimal range of inner liner modulus to achieve a high stiffness ratio.

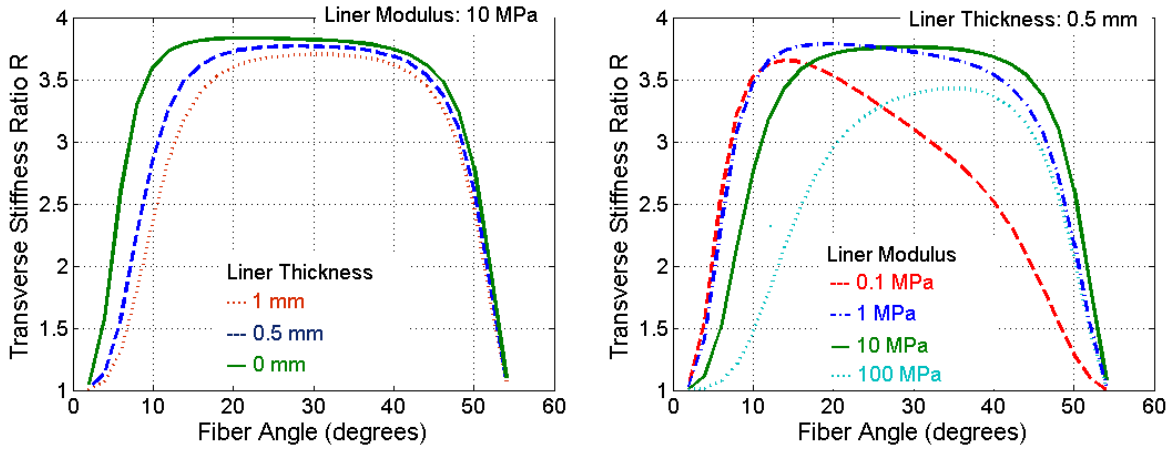

Figure 15. Parametric study of liner properties and fiber angle in F²MC tubes.

Experimental studies were performed on a sandwich beam specimen with a ±35° F²MC tube and 1 mm thick rubber inner liner (QSil 270, Quantum Silicones Inc., 8.2 MPa Young's modulus). The test specimen was mounted as a cantilever beam on which a transverse end point load is applied. Figure 16 (left) shows that the measured internal pressure values match the analytical model predictions well. The load-deflection plots obtained through the experiments are quite

linear and also match the analytical predictions well (Fig. 16, right). The measured equivalent transverse beam stiffness ratio is 3.1, as compared to 3.7 from the analytical prediction.

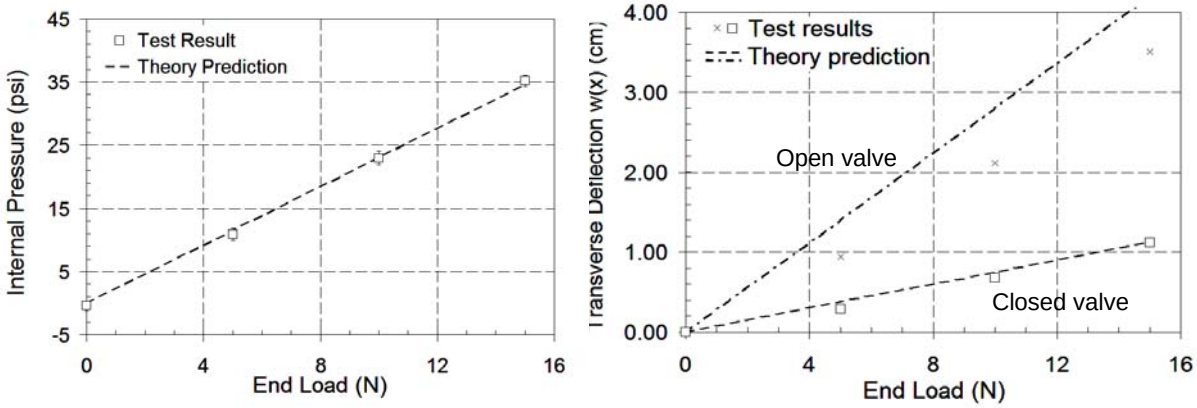

Figure 16. The internal fluid pressure with closed valve (left) and beam deflection (right) with respect to end load.

A sandwich beam with one single-segment F^{2}MC tube on a honeycomb core provides a transverse stiffness ratio of no more than 4, so the concept of tube segmentation is introduced to further improve the beam performance. The working fluid in each individual segment is independent with respect to others when the valve network is closed. Each segment can therefore be treated as an individual F^{2}MC tube upon which the single-segment analytical model can be applied. A similar parametric study is carried out to investigate the effects of different F^{2}MC designs on the beam stiffness ratio. The range of fiber angles for which the stiffness ratio is maximized is smaller compared to the single-segment tube sandwich beam (Fig. 17). The variable transverse stiffness accumulates from each segment so that the more segments in the tube, the higher the stiffness ratio. The effects of the inner liner thickness become more significant as compared to the beam with single-segment tube (Fig. 15 left and Fig. 17 right). With the same honeycomb specifications as in Table 4, a cantilever sandwich beam structure made of a 10-segment, ±25^o fiber angle F^{2}MC tube without an inner liner is capable of providing a variable transverse stiffness ratio of nearly 60. A similar sandwich beam made of a tube with a 1 mm thick inner liner (10 MPa Young's modulus) can provide a ratio of about 30.

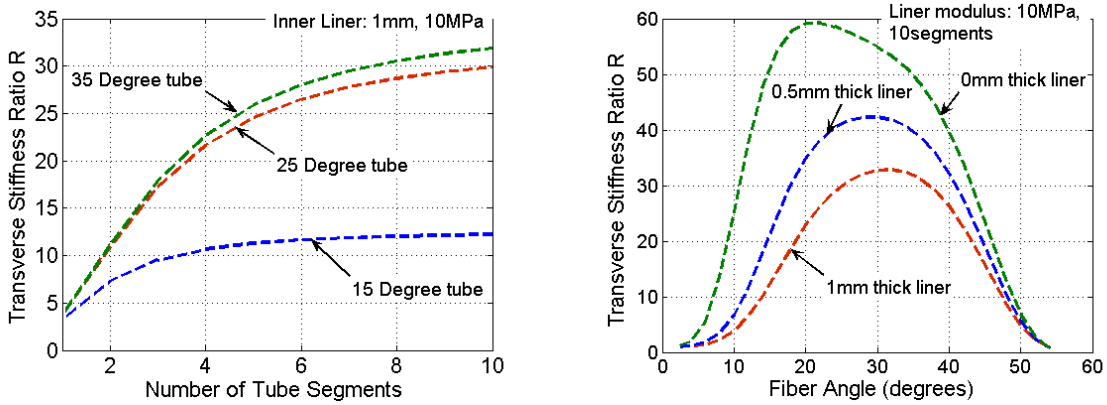

Figure 17. Parametric study results for multi-segment tubes.

Personnel Supported

The faculty members supported by this grant are Drs. Kon-Well Wang, Charles Bakis, and Chris Rahn. In addition, the project has involved one Post Doctoral Fellow Dr. Ying Shan, and two graduate students, Amir Lotfi and Suyi Li.

Publications

Y. Shan, A. Lotfi, M. Philen, S. Li, C. E. Bakis, C. D. Rahn, K.W. Wang, "Fluidic Flexible Matrix Composites for Autonomous Structural Tailoring," *SPIE Conf. on Smart Structures and Materials*, San Diego, CA, 2007.

M. Philen, Y. Shan, K. W. Wang, C. E. Bakis, C. D. Rahn, "Fluidic Flexible Matrix Composites for the Tailoring of Variable Stiffness Adaptive Structures," *AIAA/ASME/AHS Adaptive Structures Conference*, Honolulu, Hawaii, 2007.

S. Li, A. Lotfi, Y. Shan, K. W. Wang, C. D. Rahn, C. E. Bakis, "A Variable Transverse Stiffness Sandwich Structure using Fluidic Flexible Matrix Composite (F^2MC)," *SPIE Conf. on Smart Structures and Materials*, San Diego, CA, 2008.

A. Lotfi Y. Shan, S. Li, C. D. Rahn, C. E. Bakis, K. W. Wang, "Stiffness Shaping for Zero Vibration Fluidic Flexible Matrix Composites," *ASME Conference on Smart Materials, Adaptive Structures and Intelligent Systems*, Ellicott City, Maryland, 2008

Y. Shan, M. Philen, A. Lotfi, S. Li, C. E. Bakis, C. D. Rahn, K.W. Wang, "Variable Stiffness Structures Utilizing Fluidic Flexible Matrix Composites," *Journal of Intelligent Material Systems and Structures*, accepted for publication.

Honors/Awards

Dr. K. W. Wang: Fellow of the American Society of Mechanical Engineers (ASME); holder of the Diefenderfer Chair in Mechanical Engineering at Penn State; ASME 2007 N. O. Myklestad Award; ASME 2008 Adaptive Materials and Structure Prize; ASME Myklestad Award; holder of the Timoshenko Professor of Mechanical Engineering at University of Michigan. Dr. Charles Bakis: Distinguished Professor of Engineering Mechanics; Fellow of the ASME; 2006 ASC Award in Composites, American Society for Composites. Dr. Chris Rahn: Fellow of ASME; 2006 Penn State Engineering Society Outstanding Research Award.

References

1. Y. Shan, and C.E. Bakis, "Flexible Matrix Actuators," *Proc. 29th Annual Technical Conference, American Society for Composites*, Philadelphia, PA (2005).
2. Y. Shan, C.E. Bakis, M. Philen, K.W. Wang, and C.D. Rahn, "Nonlinear Finite Axisymmetric Deformation of Flexible Matrix Composite Membranes under Internal Pressure and Axial Force," *Compos. Sci. Technol.* 66, 3053-3066 (2006).

3. M. Philen, Y. Shan, P. Prakash, K.W. Wang, C.D. Rahn, A.L. Zydney, and C.E. Bakis, Fibrillar Network Adaptive Structure with Ion Transport Actuation for High Strain and Block Stress Applications," *J. Intell. Matls. Syst. Struct.*, 18, pp. 323-334 (2007).
4. M. Philen, Y. Shan, C.E. Bakis, K.W. Wang, and C.D. Rahn, "Variable Stiffness Adaptive Structure Utilizing Flexible Matrix Composites with Hydraulic Pressurization and Valve Control," *Proc. 14th AIAA/ASME/AHS Adaptive Structures Conference*, Newport, RI, (2006).
5. A.P. Boresi, R.J. Schmidt, and O.M. Siderbottom, *Advanced Mechanics of Materials*, 5th Edition, John Wiley & Sons Inc., New York, 1993.
6. S.G. Lekhnitskii, *Theory of Elasticity of an Anisotropic Body*, Holden-Day Inc., San Francisco, 1963.
7. C.T. Sun and S. Li, "Three Dimensional Effective Elastic Constants for Thick Laminates," *J. Compos. Mater.* 22, 629-645 (1988).
8. D.E. Hodgson, M.H. Wu, and R.J. Biermann, "Shape Memory Alloys," from *Metals Handbook*, ASM International, Metals Park, Ohio, Vol. 2, 10th Edition, 1990.
9. L.E. Daidley, M.J. Dapino, G.N. Washington, and T.A. Lograsso, "Modulus Increase with Magnetic Field in Ferromagnetic Shape Memory Ni-Mn-Ga," *J. Intell. Matl. Syst. Struct.* 17, 123-131 (2006).
10. C. Liu, S.B. Chun, P.T. Mather, L. Zheng, E.H. Haley, and E.B. Coughlin, "Chemically Cross-Linked Polycyclooctene: Synthesis, Characterization, and Shape Memory Behavior," *Macromolecules* 35, 9868-9874 (2002).
11. H. Tobushi, H. Hara, E. Yamada, and S. Hayashi, "Thermomechanical Properties in a Thin Film of Shape Memory Polymer of Polyurethane Series," *Proc. SPIE-The International Society for Optical Engineering*, v2716 (1996).
12. R. Kornbluh, H. Prahlad, R. Pelrine, S. Standford, M. Rosenthal, and P. von Guggenberg, "Rubber to Rigid, Clamped to Undamped: Toward Composite Materials with Wide-Range Controllable Stiffness and Damping," *Proc. SPIE-The International Society for Optical Engineering*, v5388 (2004).
13. B. Prock, T. Weisshaar, and W. Crossley, "Morphing Airfoil Shape Change Optimization with Minimum Actuator Energy as an Objective," *Proc. 9th AIAA/ISSMO Symposium on Multidisciplinary Analysis and Optimization*, Atlanta, Georgia (2002).
14. P.R. Downey, and M.J. Dapino, "Extended Frequency Bandwidth and Electrical Resonance Tuning in Hybrid Terfenol-D/PMN-PT Transducers in Mechanical Series Configuration," *J. Intell. Matl. Syst. Struct.* 16, 757-772 (2005).
15. H. Okuzaki, and K. Funasaka, "Electromechanical Properties of a Humido-Sensitive Conducting Polymer Film," *Macromolecules* 33, 8307-8311 (2000).
16. A.M. Albanese, and K.A. Cunefare, "Smart Fabric Adaptive Stiffness for Active Vibration Absorbers," *Proc. SPIE-The International Society for Optical Engineering*, v5398 (2004).
17. L.C. Davis, "Model of Magnetorheological Elastomer," *J. Appl. Phys*. 85(6), 3348-3351 (1999).
18. Ali H. Nayfeh, and P. Frank Pai, *Linear and Nonlinear Structural Mechanics*, John Wiley & Sons Inc., Hoboken, NJ, 191-192 (2004).